minerals

MDPI

Article

Mantle Evolution from Ocean to Arc: The Record in Spinel Peridotite Xenoliths in Mt. Pinatubo, Philippines

Betchaida D. Payot [1,*], Shoji Arai [2], Masako Yoshikawa [3], Akihiro Tamura [2], Mitsuru Okuno [4] and Danikko John V. Rivera [5]

1 National Institute of Geological Sciences, University of the Philippines, Diliman, Quezon City 1101, Philippines
2 Department of Earth Sciences, Kanazawa University, Kakuma, Kanazawa 920-1192, Japan; ultra_1027@yahoo.co.jp (S.A.); aking826@staff.kanazawa-u.ac.jp (A.T.)
3 Department of Earth and Planetary Systems Science, Hiroshima University, Hiroshima 739-8526, Japan; masako@hiroshima-u.ac.jp
4 Department of Earth System Science, Fukuoka University, Fukuoka 814-0180, Japan; okuno@fukuoka-u.ac.jp
5 Philippine Institute of Volcanology and Seismology, Diliman, Quezon City 1101, Philippines; danikkorivera@gmail.com
* Correspondence: bdpayot@up.edu.ph; Tel.: +63-981-8500 local 3763

Received: 3 October 2018; Accepted: 5 November 2018; Published: 8 November 2018

Abstract: A suite of peridotite xenoliths were collected from lahar flow deposits located close to the summit of Mt. Pinatubo. Spinel harzburgite is the most dominant lithology among dunites, pyroxenites and websterites. A rare spinel lherzolite xenolith (P12-7) is also present in this suite. The spinel lherzolite has well-preserved protogranular texture with very minimal presence of secondary amphibole, low Cr# in the chromian spinel, and depleted and hump shaped patterns of chondrite-normalized rare earth element (REE) patterns for the clinopyroxenes. In contrast, the spinel harzburgites contain abundant secondary amphiboles and orthopyroxenes, higher Cr# in the spinel, and slightly elevated patterns for the chondrite-normalized REE patterns for the amphiboles. The spinel lherzolite also exhibits higher olivine Fo content for a given spinel Cr# compared to the spinel harzburgites. The spinel lherzolite is interpreted as a typical residue from partial melting of abyssal peridotites whereas the spinel harzburgites may have formed via partial melting with subsequent modification during the influx of fluids in the mantle wedge. Our results suggest that fragments of MOR-derived lithosphere exist in the mantle wedge beneath the Philippine island arc. This work provides evidence for the conversion of abyssal to arc peridotites in the mantle wedge.

Keywords: xenoliths; Mt. Pinatubo; Philippines; mantle wedge; abyssal lherzolite; arc harzburgite

1. Introduction

Sandwiched between the overlying oceanic lithosphere and the subducting slab, the mantle wedge at a subduction zone is an important locus for magma generation. The nature of the mantle wedge remains to be poorly elucidated due to its location and depth. Though direct observation of the mantle wedge is not possible, information on the probable characteristics of the mantle wedge can be obtained from the mantle peridotites in obducted ophiolites [1–3], and xenoliths brought by arc lavas to the Earth's surface [4–6]. Mantle peridotites in ophiolites can be used to determine the tectonic setting in which the ophiolites were formed [7–9]. For example, the mineral chemical variations in mantle peridotites of the Oman Ophiolite point to formation at a mid-oceanic ridge [10]. Conversely, Arai and others [11] argued that the wide variability of Cr# in detrital chromian spinels from the northern portion of the Oman Ophiolite implies generation of the mantle peridotites at a fast-spreading center

but was later modified by island-arc magmatism at a subduction zone environment. Koepke and others [12] also suggested that the crustal wehrlites in the Oman Ophiolite were formed in an upper mantle wedge above a shallow subduction zone at the onset of the intraoceanic thrusting. Textural and geochemical variations in arc-derived mantle peridotite xenoliths also attest that the uppermost mantle wedge is usually metasomatized by the influx of hydrous fluids [13–17] and silicic [18,19] or adakitic melts [20]. Peridotite xenoliths exhumed from the mantle wedge beneath the Western Pacific arcs show evidence for variable metasomatic modification (e.g., hydration, silica enrichment and sulfide formation) and higher oxygen fugacity compared to abyssal peridotites [21]. The modification of pre-existing lithospheric mantle formed in a previous setting is evident from both the ophiolite and xenolith perspectives. It is therefore important to understand what is the composition of the mantle wedge prior to subduction-related alteration.

Located within a convergent plate margin, the Philippine island arc system is dominantly an amalgamation of ophiolites and ophiolitic complexes, on top of which, several volcanoes have developed through time. Despite the presence of numerous volcanoes in the Philippines, only a few localities have been identified to contain mantle xenoliths. These are the Iraya volcano in the Batan island of Batanes, the Monglo dacitic plug in Baguio and Mt. Pinatubo in western Luzon. Predominant clinopyroxene-poor spinel harzburgites along with subordinate gabbroic rocks had been documented as xenoliths in the calc-alkaline lavas and pyroclastic flows of Mt. Iraya in Batan island [4,14,15,18,22]. Serpentinized spinel dunites, amphibole-rich gabbros, amphibolites and quartz diorite are hosted by the Monglo dacite in Baguio, Northern Luzon [20,23]. Kawamoto and others [24] discussed the presence of CO_2-bearing saline fluid inclusions in spinel harzburgite xenoliths from Mt. Pinatubo. Trace element and Nd-Sr isotopic compositions of amphiboles in the Pinatubo spinel harzburgite xenoliths suggest modification due to infiltration of aqueous fluids into the mantle wedge beneath the Luzon arc [25]. In addition to these three localities, a cumulate gabbro xenolith was also reported present in the basalts to basaltic andesites of Mt. Butay in Camiguin island, northern Mindanao [26]. Given these very limited occurrences, the characteristics of the mantle wedge and deeper portions of the lower crust beneath the Philippine island arc system remains to be elucidated. In this work, new petrographic and geochemical data were generated on the spinel peridotite xenoliths hosted by Mt. Pinatubo in western Luzon. Through this study, we aim to determine the composition of the uppermost mantle beneath this segment of the Philippine island arc and the modifications it may have undergone. Lastly, the implications of our findings on the general understanding of the heterogeneous nature of the mantle wedge and its associated metasomatic processes are also discussed.

2. Geologic Background

Numerous active and inactive volcanic centers are distributed from north to south of the Philippine archipelago. The magmatism which brought about the formation of these volcanoes is intimately linked to the subduction zones present to the east and west of the Philippines. Along the western margin, the South China Sea, the Sulu Sea, and the Celebes Sea basins subduct along the Manila Trench, the Negros and Sulu Trenches, and the Cotabato Trench, respectively [27–29]. The eastern boundary is marked by the East Luzon Trough and the Philippine Trench along which the Philippine Sea Plate is subducting [30,31]. The left-lateral strike-slip Philippine Fault which cuts across the entire length of the archipelago accommodates the stress generated by the oblique convergence between the Philippine Sea Plate and the Philippine archipelago [32].

Probably known worldwide for its 1991 explosive eruption, Mt. Pinatubo is a 1459 m high stratovolcano located in western Luzon (Figure 1). Prior to its 1991 eruption, little was known about Mt. Pinatubo. It forms part of a chain of volcanoes comprising the Bataan arc front segment of the Luzon arc. Volcanism in this region of the Philippines is attributed to the eastward subduction of the South China Sea oceanic basin along the Manila Trench [33–35]. Mt. Pinatubo straddles the provinces of Zambales, Tarlac and Pampanga and is flanked to the west by the Zambales Ophiolite Complex. Mt. Pinatubo's climactic eruption on June 15, 1991 released 20 million tons of SO_2 into the

stratosphere [36,37]. Triggered by basaltic recharge into a 50 km^3 dacitic magma reservoir, the main erupted component was cummingtonite-bearing dacite (SiO_2 = 62–67 wt%) along with minor amounts of andesitic magma [38,39]. Experimental work by Prouteau and Scaillet [40] further revealed that the dacite was water-rich, oxidized and not hotter than 900 °C when it was emplaced into a shallow magma reservoir before the onset of the 1991 eruption. Moreover, the dacite was probably formed via high pressure fractionation of a hydrous and oxidized primitive basalt that crystallized amphibole and garnet upon cooling.

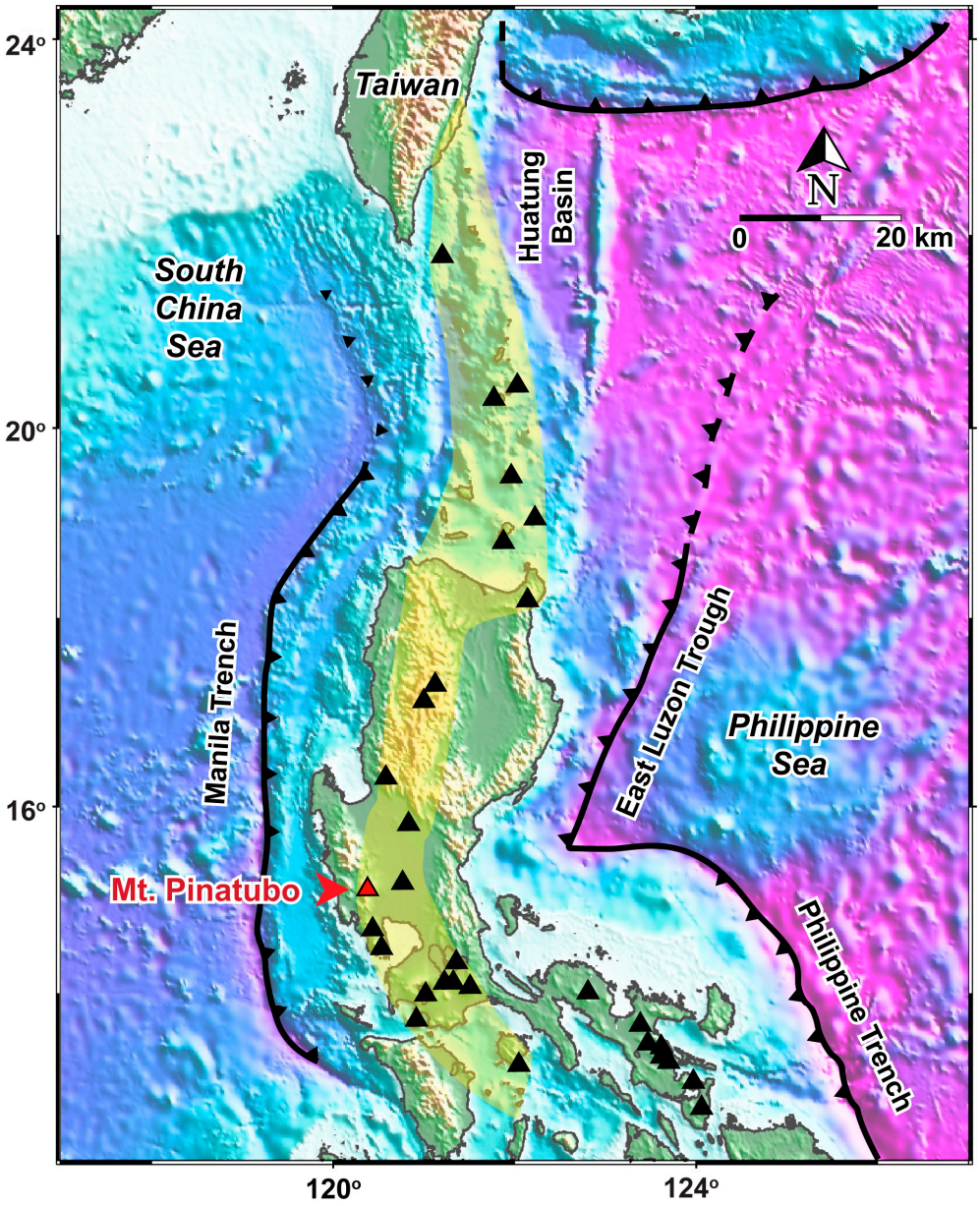

Figure 1. Map showing the location of Mt. Pinatubo (red triangle) in western Luzon. The extent of the Luzon Arc from the Coastal Range, Taiwan to northeastern Mindoro is also shown in yellow. Topographic and bathymetric map for Luzon was generated using Submap 4.1 [41].

Peridotite xenoliths occur in the lahar flow deposits located close to the summit of Mt. Pinatubo. Among the 52 samples collected, spinel harzburgite is the most dominant lithology among pyroxenites, websterites and dunites. The xenoliths are generally subrounded to subangular. The size is also variable ranging from 2 cm to as big as 35 cm across. Both coarse and fine-grained varieties of

spinel harzburgites were noted. Large brownish grains of orthopyroxene are easily identifiable in the coarse-grained spinel harzburgites (Figure 2a,b). Some of the fine-grained spinel harzburgite xenoliths are enclosed by black and thin rims of hornblendite (Figure 2c,d). More importantly, a rare spinel lherzolite (P12-7) sample is also present in this sampling suite (Figure 3a). The petrographic and geochemical characteristics of these mantle xenoliths are discussed in the succeeding sections.

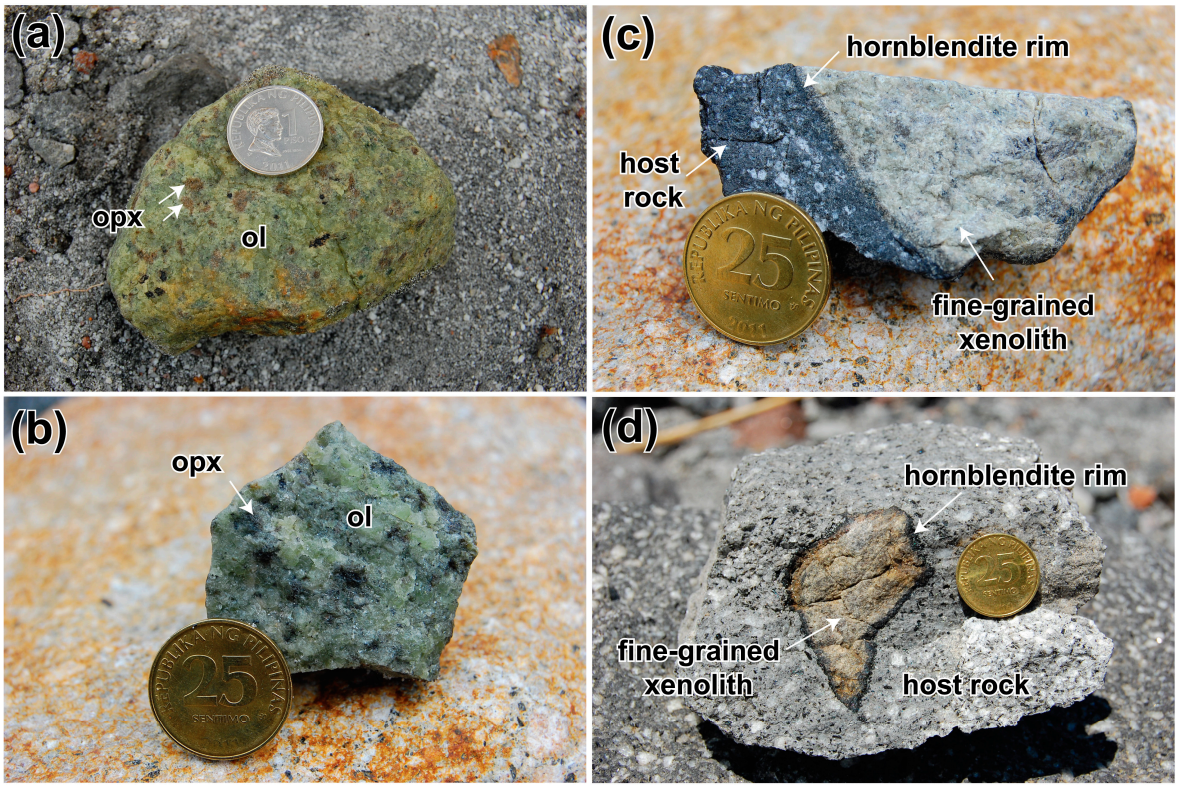

Figure 2. Mantle xenoliths in Mt. Pinatubo. (**a**,**b**) Coarse-grained spinel harzburgite xenoliths with large orthopyroxenes. (**c**,**d**) Well-preserved fine-grained spinel harzburgite xenoliths rimmed by hornblendite. Abbreviations: ol = olivine and opx = orthopyroxene. Size of coin in (**a**) is 2.3 cm and in (**c**,**d**) is 2 cm.

3. Petrography of the Mt. Pinatubo Xenoliths

The spinel lherzolite (P12-7) is coarse-grained and shows protogranular texture [42]. It is primarily composed of olivine (70%), orthopyroxene (16%), clinopyroxene (6%), chromian spinel (2%), and very minor secondary amphibole (<3%) and orthopyroxene (<3%) (Figure 3b–d). Most of the olivine grains are kink banded and contain micro-inclusions. Orthopyroxenes are large porphyroclasts with exsolution lamellae. Clinopyroxenes are turbid and subhedral to anhedral (Figure 3e,f). Vermicular and reddish brown chromian spinels are also disseminated within the sample. This spinel lherzolite piece is remarkably intact from secondary modification by melt. It has suffered far less metasomatism compared to the spinel harzburgite xenoliths. Grain boundaries of primary mantle minerals are better preserved in this spinel lherzolite sample.

The spinel harzburgite xenoliths can be classified as coarse or fine-grained. Coarse-grained xenoliths exhibit typical mantle peridotite textures while fine-grained xenoliths have minerals usually <0.1 mm in size. For this work, we selected the least metasomatized coarse-grained, spinel harzburgite xenoliths from our sampling suite which still show well-preserved mantle peridotite textures. Composed mainly of olivine (72–82%), orthopyroxene (7–16%) and chromian spinel (1–2%), the coarse-grained spinel harzburgites exhibit porphyroclastic texture (Figure 4a,b) [42]. Olivine usually shows kink banding with numerous fluid inclusion trails (Figure 4c). Primary large orthopyroxene

porphyroclasts reach up to several mm across (Figure 4d). Some orthopyroxene grains are deformed and contain exsolution lamellae of clinopyroxene. Chromian spinels are subhedral to anhedral and are commonly reddish brown. Most of the grains have a speckled appearance due to the presence of numerous holes. Fibrous secondary amphibole (2–6%) and subhedral secondary orthopyroxene (2–8%) occur in the interstices between the main mineral phases (Figure 4e,f).

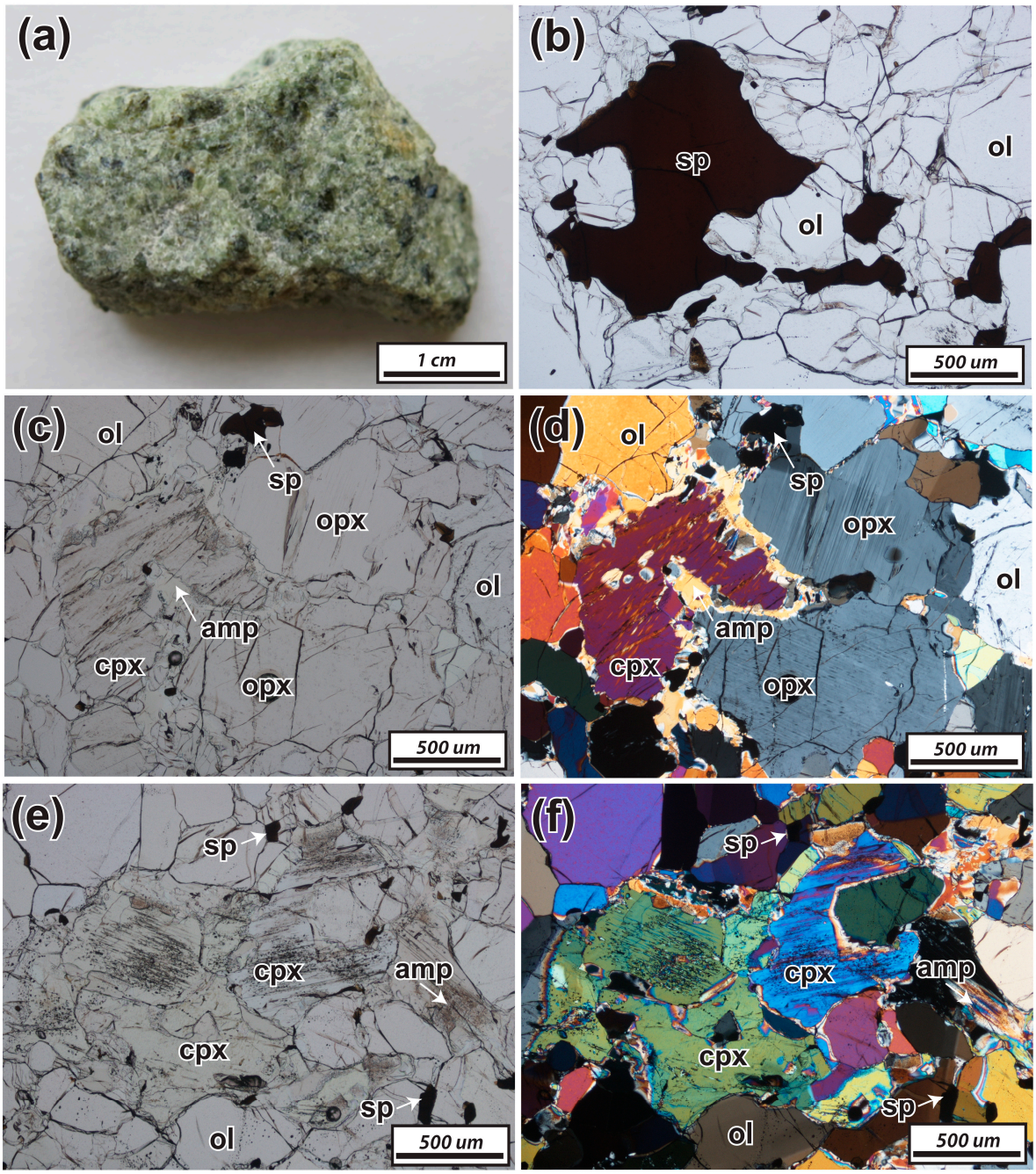

Figure 3. (**a**) Rare spinel lherzolite xenolith in Mt. Pinatubo. Photomicrographs of the spinel lherzolite xenolith: (**b–d**) The sample exhibits protogranular texture with olivine (ol), clinopyroxene (cpx), orthopyroxene (opx) and spinel (sp) as the main mineral phases. It is noteworthy that the sample is well-preserved and is free of serpentinization. (**e**,**f**) Clinopyroxene in the spinel lherzolite xenolith are often turbid, and subhedral to anhedral. Some of the clinopyroxene are partially replaced by secondary amphiboles.

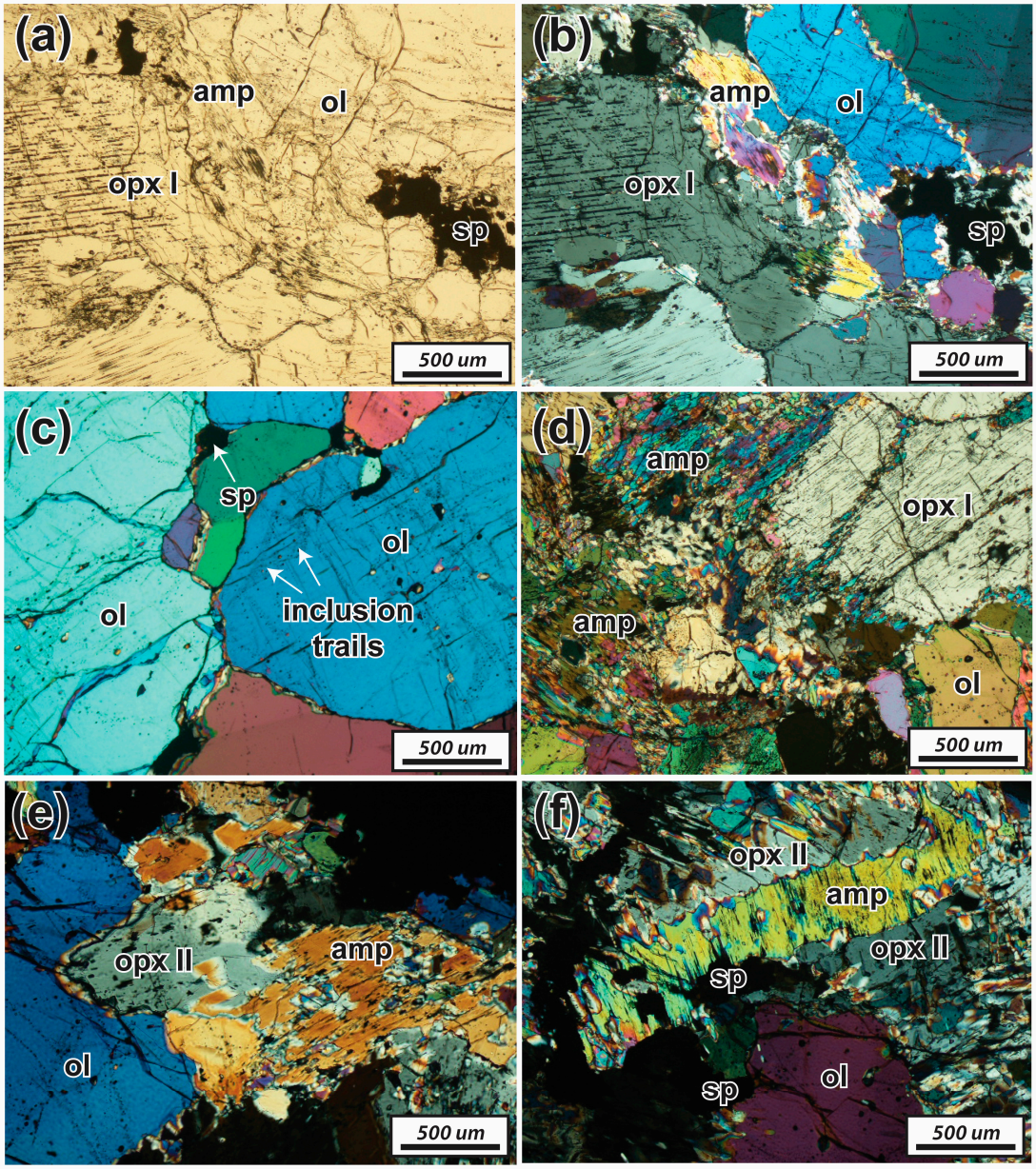

Figure 4. Photomicrographs of the coarse-grained spinel harzburgite xenoliths. (**a**,**b**) The spinel harzburgite is porphyroclastic and composed mainly of olivine (ol), orthopyroxene (opx I) and spinel (sp). (**c**) Olivine commonly contains numerous fluid inclusion trails. (**d**,**f**) Fibrous secondary amphibole (amp) and secondary orthopyroxene (opx II) commonly occur in the interstices of the main mineral phases.

4. Analytical Techniques

Major element data for the main mineral phases in the spinel peridotite xenoliths (Table S1) were obtained using an electron probe microanalyzer (EPMA, JEOL JXA 8800R) at the Kanazawa University, Japan. The following analytical conditions were used: 20 kV acceleration voltage, 20 nA probe current and 3.0 µm probe diameter. Additional microprobe data was also generated using the EPMA (JEOL JXA 8230) at the National Institute of Geological Sciences, University of the Philippines (UP-NIGS). Clinopyroxenes, amphiboles and orthopyroxenes were analyzed for trace element concentrations (Table S2) using a quadrupole inductively coupled plasma-mass spectrometer (ICP-MS) (Agilent 7500s, Yokogawa Analytical Systems) outfitted with a GeoLas Q-Plus, MicroLas laser ablation system at the Kanazawa University. Analyses were performed at 5 Hz with energy density of 8 J/cm^2 by ablating

spots of 60 µm in clinopyroxenes and amphiboles and 120 µm in orthopyroxenes. The National Institute of Standards and Technology (NIST) standard reference materials (SRM) 612 and 614 glasses were used for calibration with Si as an internal standard.

5. Geochemistry

The chromian spinels in the spinel lherzolite and harzburgite xenoliths fall within the abyssal peridotite field (Figure 5a) [7–9,43,44]. The spinel lherzolite exhibits low Cr# (<0.35) and plots within the lower end of the abyssal peridotite field. A few spinel grains in the spinel lherzolite xenolith show higher Cr#. These chromian spinels also show higher Fe^{3+} content (Figure 5b). Though there is a slight overlap, the chromian spinels in the spinel harzburgites generally shows higher Cr# than the spinel lherzolite. It can also be noted that the chromian spinels have a lower Mg# for a given Cr#. Olivine grains in the spinel lherzolite have higher Fo content (=91–92) than those in the spinel harzburgites (=90.5–91). In the olivine spinel mantle array (OSMA) of Arai [8], the spinel lherzolite distinctly plots at the higher Fo end compared to the spinel harzburgites (Figure 6a). In terms of NiO abundance, the olivine in the spinel lherzolite and harzburgites fall within the mantle olivine array (Figure 6b) [45]. Clinopyroxene which is observed only in the spinel lherzolite is diopside with substantial amounts of Cr_2O_3 reaching up to 2.21 wt%. Mg# of the clinopyroxene is high at 0.92–0.94, and Na_2O is very low (<0.08 wt%) (Figure 6c). Primary orthopyroxenes are enstatite showing high Mg# at 0.91–0.92 for the spinel lherzolite, and 0.90–0.91 for the spinel harzburgites. Amphiboles are tremolite and magnesiohornblende with very high Mg#, 0.93–0.96 in the spinel lherzolite, and 0.91–0.95 in the spinel harzburgites. Al_2O_3 wt% in the tremolite and magnesiohornblende varies from 1–8 wt%.

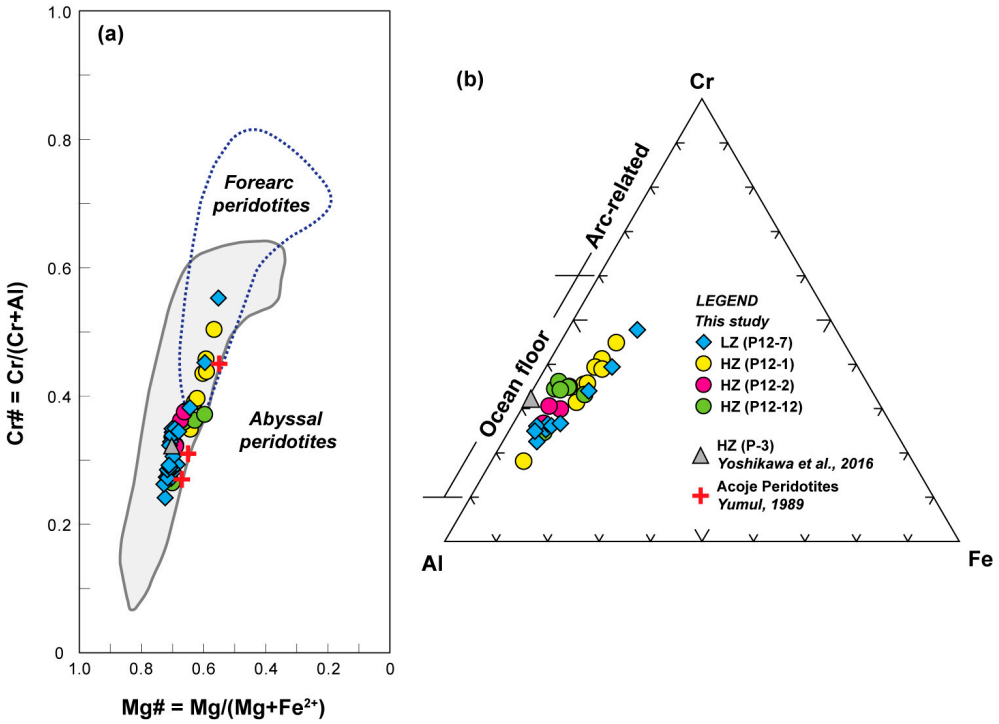

Figure 5. (**a**) Cr# vs Mg# of chromian spinels in the Mt. Pinatubo spinel peridotite xenoliths. Data for the least metasomatized coarse-grained, spinel harzburgite xenolith from Mt. Pinatubo reported by Yoshikawa et al. [25] is indicated by the gray triangle. Red crosses (+) are chromian spinel data of the Acoje peridotites of the Zambales Ophiolite Complex [46]. Abyssal peridotite [43] and forearc peridotite fields [9,44] are also shown. (**b**) Ternary diagram showing the Cr-Al-Fe^{3+} content in the chromian spinels in the Mt. Pinatubo spinel peridotite xenoliths. Note that a few of the chromian spinels in the spinel lherzolite plot toward the Fe-rich end of the diagram. Abbreviations: LZ = spinel lherzolite and HZ = spinel harzburgite.

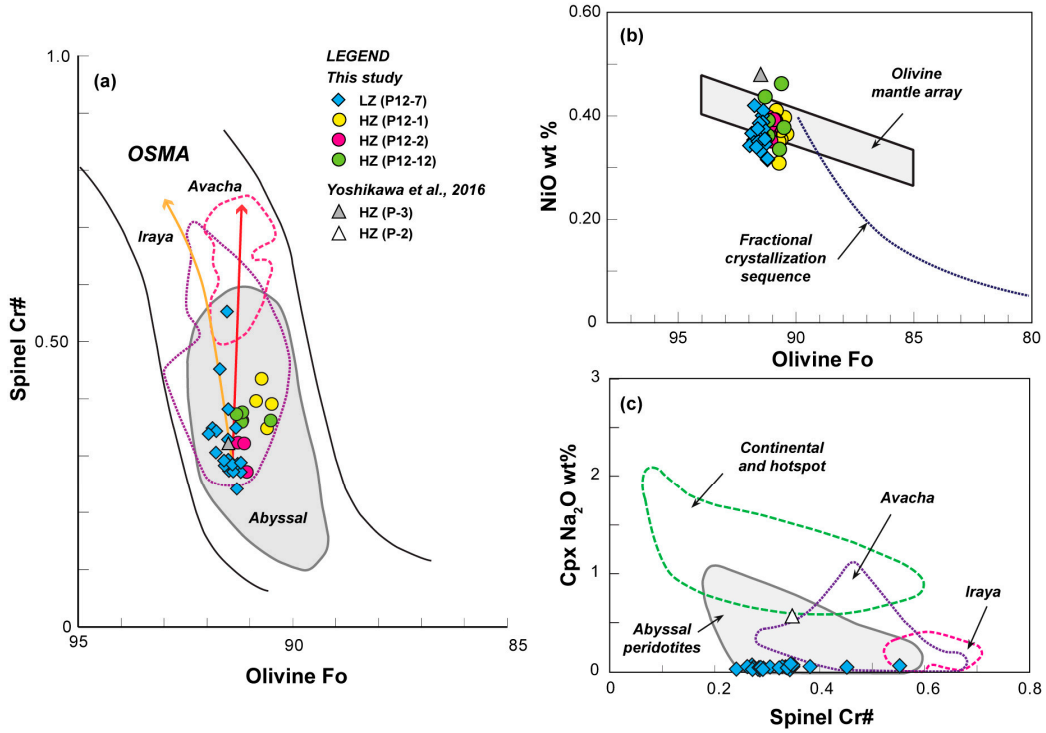

Figure 6. (**a**) Olivine forsterite vs spinel Cr#. The Mt. Pinatubo spinel peridotite xenoliths plot within the olivine spinel mantle array (OSMA) [8]. The spinel lherzolite (LZ) shows higher Fo content for a given Cr# compared to the spinel harzburgites (HZ). Abyssal peridotite [8], and Avacha and Iraya fields [21] are also shown. The orange arrow indicates the residual trend for spinel peridotites [8] while the red arrow defines the trend for the Avacha peridotite xenoliths [21]. (**b**) Olivine forsterite versus NiO wt%. The Mt. Pinatubo spinel lherzolite and harzburgite xenoliths plot within the olivine mantle array [45]. The fractional crystallization trend is after Sato [47]. (**c**) Spinel Cr# vs Cpx Na_2O. The clinopyroxenes in the spinel lherzolite xenolith from Mt. Pinatubo show very low Na_2O content. References for the different fields are as follows: abyssal, continental and hotspot [48], Avacha [21] and Iraya [4,18].

Chondrite-normalized trace element patterns for clinopyroxenes and amphiboles in the Mt. Pinatubo spinel peridotite xenoliths are shown in Figure 7. The clinopyroxenes generally exhibit hump-shaped patterns with little variation in trace element abundances (Figure 7a). The light rare earth elements (LREEs) are distinctly depleted. A steep slope is observed from the LREEs to the middle rare earth elements (MREEs) and to the relatively flat-lying patterns of the heavy rare earth elements (HREEs). Depletion in Zr and enrichment in Sr is also evident in the extended trace element diagram (Figure 7b). The amphiboles in the spinel lherzolite typically show spoon-shaped patterns with slight enrichment in the LREEs. The amphiboles in the spinel harzburgites display similar patterns but with higher and distinct enrichment in the LREEs (Figure 7c). One sample (P12-12) particularly shows higher LREE content at least 10x higher than that of the amphiboles in the spinel lherzolite. Except for sample P12-12, pronounced Sr and Ti positive anomalies and slight enrichment in Zr is also observed in the extended trace element patterns (Figure 7d) of the amphiboles in the spinel lherzolites and harzburgites.

6. Equilibrium Conditions and Oxygen Fugacity

Employing the pyroxene geothermometer of Wells [49] which is based on the mutual solubility of Ca and Mg and Fe/Mg partitioning between coexisting clinopyroxene and orthopyroxene, estimated temperatures for the spinel lherzolite xenolith is within the range of 867–906 °C. Clinopyroxene was not observed in the spinel harzburgite xenoliths. The olivine-orthopyroxene-spinel oxygen barometer

by Ballhaus et al. [50] was also used to estimate the oxidation state of the Mt. Pinatubo xenoliths. Assuming 1.5 GPa, the calculated oxygen fugacity for both spinel lherzolites and harzburgites is high with [$\Delta\log(fO_2)$FMQ = +0.3 to +2.2]. These values are distinctively higher than that of typical abyssal peridotites [$\Delta\log(fO_2)$FMQ = −2.5 to +1.0 [51], and $\Delta\log(fO_2)$FMQ = −0.47 to +0.07 [52]] but are comparable to the redox state of highly oxidized peridotite xenoliths from central Mexico [$\Delta\log(fO_2)$FMQ = 1.5 to +2.4; [53]] and arc peridotites [$\Delta\log(fO_2)$FMQ = 0.3 to +2.0 [54]].

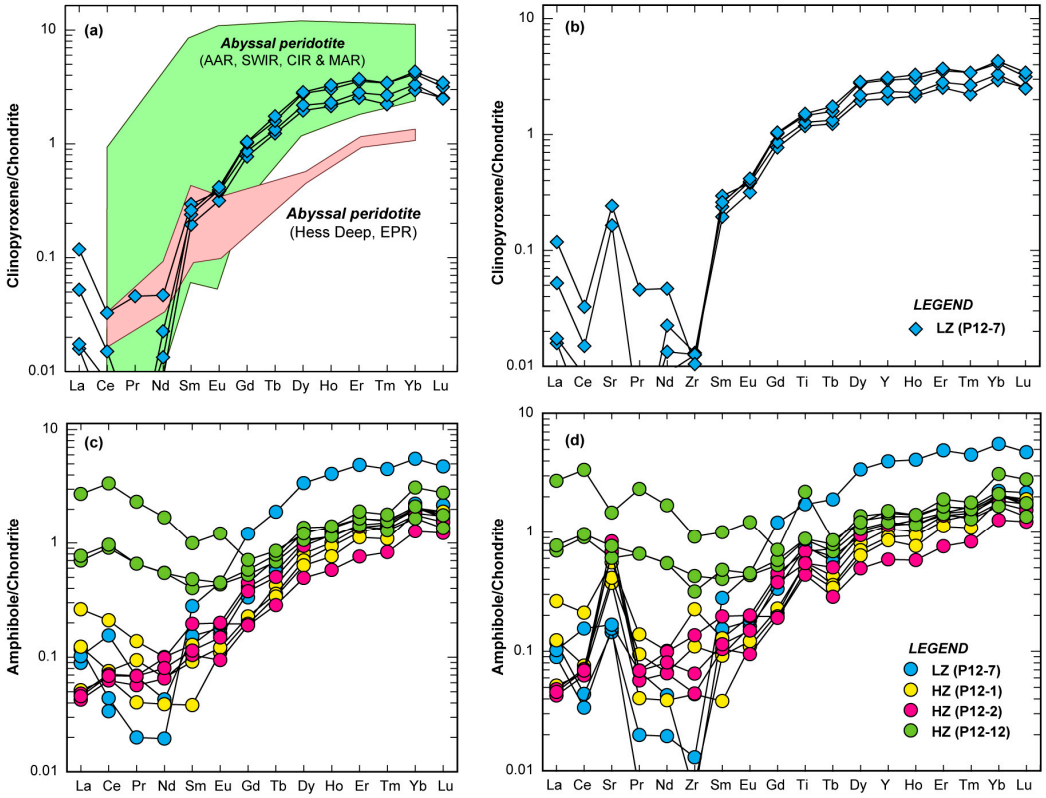

Figure 7. (**a**) Chondrite-normalized rare earth element (REE) patterns for clinopyroxenes in the spinel lherzolite (LZ) xenolith. The hump-shaped pattern of the clinopyroxene is similar to that of clinopyroxenes in abyssal peridotites from slow-spreading mid-oceanic ridges. (**b**) Positive Sr and negative Zr anomalies are evident in the clinopyroxenes in the spinel lherzolite xenolith. (**c**) Chondrite-normalized REE patterns for amphiboles in both the spinel lherzolite and harzburgite (HZ) xenoliths are also hump-shaped. However, variable enrichment in the light REEs (LREEs) can be noted. (**d**) The amphiboles in the spinel lherzolite and harzburgite xenoliths generally show Sr and Ti positive anomalies in the extended trace element diagram. Chondrite normalization values are from Sun and McDonough [55]. References for abyssal peridotite data are as follows: American Antarctic Ridge (AAR) and Southwest Indian Ridge (SWIR) [56,57], Central Indian Ridge (CIR) [58,59], Mid-Atlantic Ridge (MAR) [60,61] and East Pacific Rise (EPR) [62].

7. Discussion

7.1. Characterization of the Mt. Pinatubo Spinel Peridotite Xenoliths

Arc-derived peridotite xenoliths are relatively rare compared to mantle peridotite samples from other tectonic settings [18,63]. In the Philippines, spinel harzburgite was the main type of xenolith in Mt. Iraya in Batan island [4,14,15,18,22]. Though very rare in occurrence, the lone spinel lherzolite xenolith in our sample suite is a very important piece. The coarse-grained spinel lherzolite from Mt. Pinatubo is remarkably fresh with well-preserved mantle peridotite texture and grain boundaries (Figure 3). Its mineralogy comprised of olivine, clinopyroxene, orthopyroxene and spinel is typical of abyssal spinel peridotites. In contrast, the spinel harzburgite xenoliths may have experienced modification as

indicated by the abundance of secondary finer grains of orthopyroxenes and amphiboles in the samples (Figure 4). The formation of secondary orthopyroxenes is related to the interaction of mantle wedge peridotites with aqueous fluids from the subducted slab [25]. Formation of secondary or metasomatic orthopyroxene due to the reaction of primary olivine with the infiltration of SiO_2-rich melts or fluids was also prevalent in the Avacha peridotite xenoliths in the Kamchatka arc [64,65]. Clinopyroxenes and amphiboles closely associated with the metasomatic orthopyroxenes are also believed to be of metasomatic origin, having been precipitated from, or modified by metasomatic fluids or melts [65]. In the case of the Lihir xenoliths, hydrous metasomatism of the oceanic sub-arc mantle led to the formation of veins within mantle harzburgite xenoliths. The secondary mineral assemblage consists of fibrous, radiating orthopyroxene and fine-grained Fe-Ni sulfide with minor olivine, clinopyroxene, phlogopite, amphibole and magnetite [66,67].

The Cr# of the chromian spinel in the spinel lherzolite and harzburgites is within the range for abyssal peridotites (Figure 5a). The Cr# of chromian spinel is an effective indicator of the degree of partial melting undergone by mantle peridotites. Fertile low-Cr/Al peridotites are characterized by spinel lherzolite mineral assemblages, with or without plagioclase, indicating their derivation within or at the low-pressure limit of the spinel lherzolite stability field [21]. Chromian spinels in lherzolites, harzburgites, dunites and plagioclase-bearing peridotites from abyssal settings have Cr# ranging from 0.10 to 0.60 with the more fertile lherzolites having spinel Cr# dominantly <0.30 [7,8]. A few spinel grains in the spinel lherzolite shows high Cr# (>0.38) but these grains also show higher Fe^{3+} content (Figure 5b). These spinel grains are locally surrounded by finer grains of secondary orthopyroxene and amphibole unlike the low Cr# (<0.35) chromian spinels which are located between olivines and pyroxenes. Using olivine Fo versus spinel Cr#, the spinel lherzolite and harzburgites plot within the olivine spinel mantle array (Figure 6a). The NiO wt% range of the olivines in the spinel lherzolite and harzburgites also fall within the olivine mantle array (Figure 6b). However, the spinel lherzolite clearly shows higher Fo content for a given Cr# compared to the spinel harzburgites. The spinel lherzolite follows the residual trend for anhydrous spinel peridotites [8] whereas the spinel harzburgites deviate away from this trend and follows the trend for the Avacha peridotite xenoliths (Figure 6a). These trends indicate that the spinel lherzolite xenolith is a typical residue from partial melting of peridotites possibly at an abyssal setting whereas the spinel harzburgite xenoliths may have formed from partial melting with subsequent modification during the influx of fluids in the mantle wedge.

The low Cr# of spinel in the spinel lherzolite is also coupled with low Na_2O content in the clinopyroxenes (Figure 6c). The clinopyroxene in the spinel lherzolite shows significantly lower Na_2O content compared to the clinopyroxene in the spinel harzburgite xenolith (P-2) of Yoshikawa et al. [25]. The relationship between the Cr# of chromian spinel, which is a good indicator of the degree of depletion, and the Na content, which is mainly representative of the jadeite component of the coexisting clinopyroxene can be used as a possible measure of pressure of melting [48]. The relative low Na content of the clinopyroxenes at a given Cr# of spinel in the Mt. Pinatubo spinel lherzolite is similar to the reported low values in the Western Pacific peridotite xenoliths and abyssal peridotites [21]. This geochemical feature is believed to be indicative of melting at relatively low pressure.

Trace elements in clinopyroxene which is one of the key minerals during mantle melting, provide an efficient way to determine the degree of depletion undergone by mantle peridotites. Clinopyroxenes in abyssal peridotites especially from the slow-spreading ridges such as the American Antarctic Ridge (AAR), Southwest Indian Ridge (SWIR), Central Indian Ridge (CIR) and the Mid-Atlantic Ridge (MAR) often show hump-shaped patterns with distinct depletion in LREEs [56–61]. These depleted patterns in the clinopyroxenes in abyssal peridotites are attributed to varying degrees of partial melting in the spinel or garnet peridotite fields. The chondrite-normalized REE patterns of the clinopyroxenes in the Mt. Pinatubo spinel lherzolite xenoliths is hump-shaped and plots in the depleted portion of the abyssal peridotite field (Figure 7). This LREE-depleted pattern of the clinopyroxenes in the spinel lherzolite xenolith clearly shows that this spinel lherzolite is residual material after melt extraction

beneath a mid-oceanic ridge. The positive Sr anomaly relative to the LREEs can be possibly attributed to post-melting processes.

7.2. Possible Origin of the Mt. Pinatubo Spinel Peridotite Xenoliths

Mt. Pinatubo is flanked to the west by the Zambales Ophiolite Complex (ZOC). The ZOC is composed of three massifs: the Masinloc, Cabangan and San Antonio which are distributed from north to south. The Masinloc massif can be further subdivided into the Acoje and Coto blocks. The Acoje block is characterized by lherzolite-harzburgite, a kilometer-thick transition zone dunite, a well-developed layered ultramafic (e.g., clinopyroxenite, wehrlite, websterite) and mafic (e.g., gabbronorite, norite) cumulate sequence and a volcanic-hypabyssal unit with a crystallization order of olivine/spinel > clinopyroxene > orthopyroxene > plagioclase. On the other hand, the Coto block consists of a harzburgite, a thin transition zone dunite, a layered gabbro-troctolite unit and a volcanic-hypabyssal suite with a crystallization order of olivine/spinel > plagioclase > clinopyroxene > orthopyroxene [68]. Petrological and geochemical data have established that the Acoje block is of island arc origin whereas the Coto block is representative of a transitional mid-oceanic ridge (MOR) to island arc setting [46,69]. Conversely, some workers have argued that the Acoje and Coto blocks physically belong to a single unit and the compositional difference between the two is due to the variation in the source mantle rocks [70].

The Cr# of the chromian spinels of the Mt. Pinatubo spinel peridotites is comparable to the Cr# of chromian spinels in the residual spinel peridotites of the Acoje block of the ZOC (Figure 5). However, the Mg# of the chromian spinels of the Mt. Pinatubo spinel peridotite xenoliths are slightly higher than the Acoje residual peridotites. This suggests that the Mt. Pinatubo spinel peridotite xenoliths were equilibrated at a higher temperature than the residual peridotites of the Acoje block [71]. This also implies that the Mt. Pinatubo xenoliths may have been sourced from greater depths than the Acoje residual peridotites. The presence of fertile spinel lherzolites has also been reported from the mantle section of the Cretaceous Isabela Ophiolite exposed in northeastern Luzon [72]. Spinel lherzolites of the Isabela Ophiolite show very low Cr# (~0.08–0.16) in the chromian spinels, and hump-shaped and depleted patterns for the clinopyroxenes. Given these characteristics, which are akin to abyssal peridotites, the Isabela Ophiolite is interpreted to have formed in a slow-spreading mid-oceanic ridge. The occurrence of residual abyssal peridotites in the ZOC and the Isabela Ophiolite imply that MOR-derived mantle peridotites are preserved within the Philippine island arc system. Present day oceanic basins surrounding the Philippines are generally younger than Cretaceous which is the reported age for most of the Philippine ophiolites and ophiolitic complexes [29]. Moreover, most of these ophiolites and ophiolitic complexes are thought to have originated from supra-subduction zone related oceanic basins such as the proto-South China Sea plate and the proto-Philippine Sea plate while some may have formed from mature marginal basins [73]. The ophiolitic substratum of Northern Luzon have also been postulated to have the same origin of the Early Cretaceous Huatung Basin located to the east of present day Taiwan. However, the thickness of the crust (~12 km) beneath the Huatung Basin, and the regular topography of the basement and its relatively smooth relief imply generation at a fairly fast and constant spreading rate of 5 to 6 cm/yr [74]. The possible presence of a slow-spreading ridge derived oceanic lithosphere beneath Luzon island needs to be further ascertained.

The Mt. Pinatubo spinel lherzolite with distinct abyssal characteristics is probably the "original" material in the uppermost mantle beneath the Luzon Arc (Figure 8). Subsequent subduction initiation and infiltration of fluids into the mantle wedge resulted to the partial melting and modification of the spinel lherzolite forming spinel harzburgites. This is supported by the amphiboles in the Pinatubo spinel harzburgite xenoliths which show enrichment in fluid-mobile elements, such as Rb, Ba, U, Pb and Sr, and Nd-Sr isotopic ratios compared to mantle values [25]. The high oxygen fugacities in the spinel peridotite xenoliths also attest to this occurrence. The mantle wedge in subduction zones are highly oxidized relative to oceanic mantle [53,54]. The intensity of metasomatism in the mantle wedge could be variable such that fragments of the spinel lherzolites may have remained intact and

unaltered. Both unaltered spinel lherzolite and metasomatized spinel harzburgites are then extruded rapidly to the surface as xenoliths by the basaltic magma, which eventually caused the 1991 eruption of Mt. Pinatubo. The Mt. Pinatubo spinel peridotite xenoliths therefore provide a record of the conversion of oceanic to arc peridotites via partial melting and interaction or infiltration of fluids in the mantle wedge.

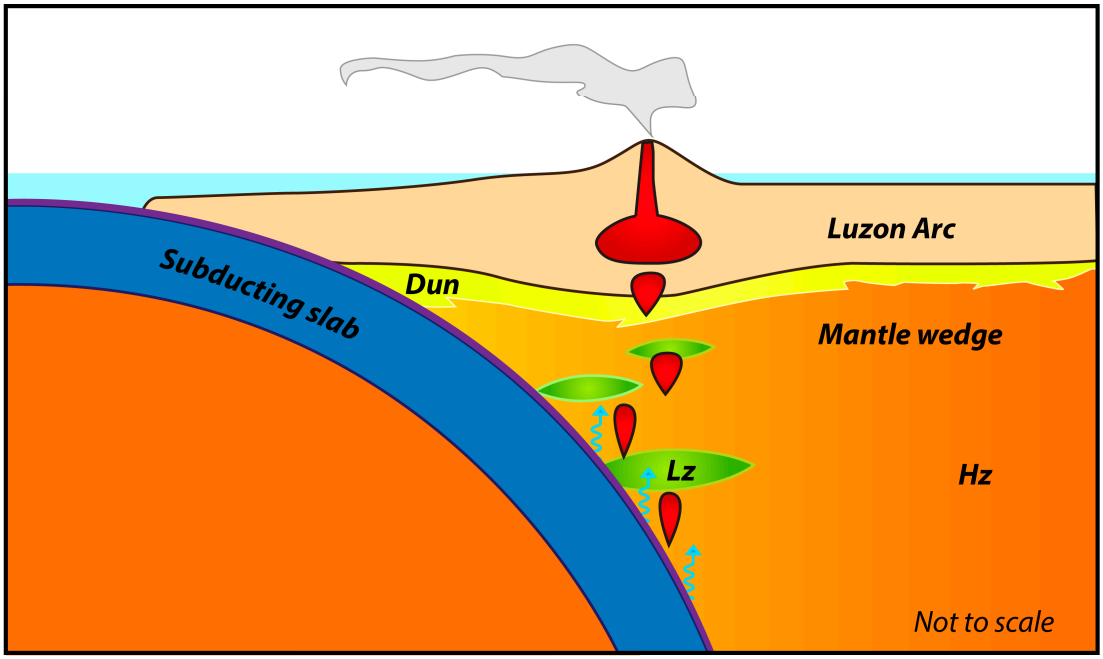

Figure 8. Diagram depicting the origin of the Mt. Pinatubo spinel peridotite xenoliths. Spinel lherzolite were converted to spinel harzburgite due to infiltration of fluids and partial melting in the mantle wedge. Lz = spinel lherzolite, Hz = spinel harzburgite and Dun = dunite.

8. Conclusions

Spinel peridotite xenoliths are hosted by the Mt. Pinatubo dacites in western Luzon. Spinel harzburgite is the most common rock type among dunites, pyroxenite and websterites. The highlight of this sampling set is a rare coarse-grained spinel lherzolite xenolith (P12-7), which shows well-preserved mantle peridotite textures. The petrographic and geochemical characteristics of the spinel lherzolite xenolith are indicative of an abyssal origin. The spinel lherzolite was converted to spinel harzburgite due to the influx of fluids and partial melting in the mantle wedge. The occurrence of this rare spinel lherzolite implies that fragments of MOR-derived lithosphere exist in the mantle wedge beneath the Philippine island arc system. This work also provides evidence for the modification of abyssal to arc peridotites in the mantle wedge.

Supplementary Materials: The following are available online at http://www.mdpi.com/2075-163X/8/11/515/s1, Table S1: Mineral chemistry of the olivine, clinopyroxene, orthopyroxene, spinel and amphibole in the Mt. Pinatubo spinel peridotite xenoliths. Table S2: Trace element abundances for clinopyroxenes and amphiboles in the Mt. Pinatubo spinel lherzolite and harzburgite xenoliths.

Author Contributions: B.D.P. is the principal author and conducted the field sampling, laboratory analyses and preparation of the manuscript. S.A. is the main supervisor of this work, providing funding and guidance from the inception of the study to the review and editing of this manuscript. M.Y., M.O. and D.J.V.R participated in the field sampling and discussions on the petrogenesis of the xenoliths. A.T. helped in the generation geochemical data.

Funding: This research was partly funded by the PhD Incentive Award granted to the first author by the Office of the Vice Chancellor for Research and Development (OVCRD), University of the Philippines, Diliman (UP Diliman).

Acknowledgments: The authors would like to thank the Rushurgent Working Group of UP Diliman for providing logistical support during the fieldwork. Support provided by the local government units of Capas, Tarlac, and Botolan, Zambales is highly appreciated. Comments by three anonymous reviewers helped improved the quality of this paper.

Conflicts of Interest: The authors declare no conflict of interest.

References

1. Ozawa, K. Melting and melt segregation in the mantle wedge above a subduction zone: Evidence from the chromite-bearing peridotites of the Miyamori ophiolite complex, northeastern Japan. *J. Petrol.* **1994**, *35*, 647–678. [CrossRef]
2. Jean, M.; Shervais, J.W. The distribution of fluid mobile and other incompatible trace elements in orthopyroxene from mantle wedge peridotites. *Chem. Geol.* **2017**, *457*, 118–130. [CrossRef]
3. Prigent, C.; Guillot, S.; Agard, P.; Lemarchand, D.; Soret, M.; Ulrich, M. Transfer of subduction fluids into the deforming mantle wedge during nascent subduction: Evidence from trace elements and boron isotopes (Semail ophiolite, Oman). *Earth Planet. Sci. Lett.* **2018**, *484*, 213–228. [CrossRef]
4. Arai, S.; Kida, M. Origin of fine-grained peridotite xenoliths from Iraya volcano of Batan Island, Philippines: Deserpentinization or metasomatism at the wedge mantle beneath an incipient arc? *Isl. ARC* **2000**, *9*, 458–471. [CrossRef]
5. Satsukawa, T.; Godard, M.; Demouchy, S.; Michibayashi, K.; Ildefonse, B. Chemical interactions in the subduction factory: New insights from an in situ trace element and hydrogen study of the Ichinomegata and Oki-Dodo mantle xenoliths (Japan). *Geochim. Cosmochim. Acta* **2017**, *208*, 234–267. [CrossRef]
6. Polat, A.; Frei, R.; Longstaffe, F.J.; Thorkelson, D.J.; Friedman, E. Petrology and geochemistry of the Tasse mantle xenoliths of the Canadian Cordillera: A record of Archean to Quaternary mantle growth, metasomatism, removal, and melting. *Tectonophysics* **2018**, *737*, 1–26. [CrossRef]
7. Dick, H.J.B.; Bullen, T. Chromian spinel as indicator in abyssal and alpine-type peridotites and spatially associated lavas. *Contrib. Mineral. Petr.* **1984**, *86*, 54–76. [CrossRef]
8. Arai, S. Characterization of spinel peridotites by olivine-spinel compositional relationships: Review and interpretation. *Chem. Geol.* **1994**, *113*, 191–204. [CrossRef]
9. Parkinson, I.J.; Pearce, J.A. Peridotites from the Izu-Bonin-Mariana forearc (ODP Leg 125): Evidence for mantle melting and melt-mantle interaction in a supra-subduction zone setting. *J. Petrol.* **1998**, *39*, 1577–1618. [CrossRef]
10. Le Mee, L.; Girardeau, J.; Monnier, C. Mantle segmentation along the Oman Ophiolite fossil mid-ocean ridge. *Nature* **2004**, *282*, 58–61.
11. Arai, S.; Kadoshima, K.; Morishita, T. Widespread arc-related melting in the mantle section of the northern Oman ophiolite as inferred from detrital chromian spinels. *J. Geol. Soc. Lond.* **2006**, *163*, 869–879. [CrossRef]
12. Koepke, J.; Schoenborn, S.; Oelze, M.; Wittman, H.; Feig, S.T.; Hellebrand, E.; Boudier, F.; Schoenberg, R. Petrogenesis of crustal wehrlites in the Oman ophiolite: Experiments and natural rocks. *Geochem. Geophys. Geosyst.* **2009**, *10*, Q10002. [CrossRef]
13. Tatsumi, Y.; Hamilton, D.L.; Nesbitt, R.W. Chemical characteristics of fluid phase released from a subducted lithosphere and origin of arc magmas: Evidence from high-pressure experiments and natural rocks. *J. Volcanol. Geotherm. Res.* **1986**, *29*, 293–309. [CrossRef]
14. Vidal, P.; Dupuy, C.; Maury, R.; Richard, C. Mantle metasomatism above subduction zones: Trace-element and radiogenic isotope characteristics of peridotite xenoliths from Batan Island (Philippines). *Geology* **1989**, *17*, 1115–1118. [CrossRef]
15. Maury, R.C.; Defant, M.J.; Joron, J.-L. Metasomatism of the sub-arc mantle inferred from trace elements in Philippine xenoliths. *Nature* **1992**, *360*, 661–663. [CrossRef]
16. Facer, J.; Downes, H.; Beard, A. In situ serpentinization and hydrous fluid metasomatism in spinel dunite xenoliths from the Bearpaw Mountains, Montana, USA. *J. Petrol.* **2009**, *50*, 1443–1475. [CrossRef]
17. Neumann, E.-R.; Abu El-Rus, M.A.; Tiepolo, M.; Ottolini, L.; Vannucci, R.; Whitehouse, M. Serpentinization and deserpentinization reactions in the upper mantle beneath Fuerteventura revealed by peridotite xenoliths with fibrous orthopyroxene and mottled olivine. *J. Petrol.* **2015**, *56*, 3–31. [CrossRef]

18. Arai, S.; Takada, S.; Michibayashi, K.; Kida, M. Petrology of peridotite xenoliths from Iraya volcano, Philippines, and its implication for dynamic mantle-wedge process. *J. Petrol.* **2004**, *45*, 369–389. [CrossRef]
19. Ishimaru, S.; Arai, S. Calcic amphiboles in peridotite xenoliths from Avacha volcano, Kamchatka, and their implications for metasomatic conditions in the mantle wedge. *J. Geol. Soc. Lond.* **2008**, *293*, 35–55. [CrossRef]
20. Gregoire, M.; Jego, S.; Maury, R.C.; Polve, M.; Payot, B.D.; Tamayo, R.A., Jr.; Yumul, G.P., Jr. Metasomatic interactions between slab-derived melts and depleted mantle: Insights from xenoliths within Monglo adakite (Luzon arc, Philippines). *Lithos* **2008**, *103*, 415–430. [CrossRef]
21. Arai, S.; Ishimaru, S. Insights into petrological characteristics of the lithosphere of mantle wedge beneath arcs through peridotite xenoliths: A review. *J. Petrol.* **2008**, *49*, 665–695. [CrossRef]
22. Richard, M.; Maury, R.; Bellon, H.; Stephan, J.F.; Boirat, J.M.; Calderon, A. Geology of Mt. Iraya volcano and Batan Island, northern Philippines. *J. Volcanol.* **1986**, *3*, 1–27.
23. Payot, B.D.; Jego, S.; Maury, R.; Polve, M.; Gregoire, M.; Ceuleneer, C.; Tamayo, R.A., Jr.; Yumul, G.P., Jr.; Bellon, H.; Cotten, J. The oceanic substratum of Northern Luzon: Evidence from xenoliths within Monglo adakite (the Philippines). *Isl. ARC* **2007**, *16*, 276–290. [CrossRef]
24. Kawamoto, T.; Yoshikawa, M.; Kumagai, Y.; Mirabueno, M.H.T.; Okuno, M.; Kobayashi, T. Mantle wedge infiltrated with saline fluids from dehydration and decarbonation of subducting slab. *Proc. Natl. Acad. Sci. USA* **2013**, *24*, 9663–9668. [CrossRef] [PubMed]
25. Yoshikawa, M.; Tamura, A.; Arai, S.; Kawamoto, T.; Payot, B.D.; Rivera, D.J.; Bariso, E.B.; Mirabueno, M.H.T.; Okuno, M.; Kobayashi, T. Aqueous fluids and sedimentary melts as agents for mantle wedge metasomatism as inferred from peridotite xenoliths at Pinatubo and Iraya volcanoes, Luzon arc, Philippines. *Lithos* **2016**, *262*, 355–368. [CrossRef]
26. Castillo, P.R.; Janney, P.E.; Solidum, R.U. Petrology and geochemistry of Camiguin Island, southern Philippines: Insights to the source of adakites and other lavas in a complex arc setting. *Contrib. Mineral. Petrol.* **1999**, *134*, 33–51. [CrossRef]
27. Hayes, D.E.; Lewis, S.D. A geophysical study of the Manila Trench, Luzon, Philippines 1. Crustal structure, gravity, and regional tectonic evolution. *J. Geophys. Res.* **1984**, *89*, 9171–9195. [CrossRef]
28. Rangin, C. The Philippine Mobile Belt: A complex plate boundary. *J. Southeast Asian Earth Sci.* **1991**, *6*, 209–220. [CrossRef]
29. Yumul, G.P., Jr.; Dimalanta, C.B.; Tamayo, R.A., Jr.; Maury, R.C. Collision, subduction and accretion events in the Philippines: A synthesis. *Isl. ARC* **2003**, *12*, 77–91. [CrossRef]
30. Lallemand, S.E.; Popoff, M.; Cadet, J.-P.; Bader, A.-G.; Pubellier, M.; Rangin, C.; Deffontaines, B. Genetic relations between the central and southern Philippine Trench and the Sangihe Trench. *J. Geophys. Res.* **1998**, *103*, 933–950. [CrossRef]
31. Ozawa, A.; Tagami, T.; Listanco, E.L.; Arpa, C.B.; Sudo, M. Initiation and propagation of subduction along the Philippine Trench: Evidence from the temporal and spatial distribution of volcanoes. *J. Asian Earth Sci.* **2004**, *23*, 105–111. [CrossRef]
32. Aurelio, M.A. Shear partitioning in the Philippines: Constraints from Philippine Fault and global positioning system data. *Isl. ARC* **2000**, *9*, 584–597. [CrossRef]
33. Defant, M.J.; Jacques, D.; Maury, R.C.; De Boer, J.; Joron, J.L. Geochemistry and tectonic setting of the Luzon arc, Philippines. *Geol. Soc. Am. Bull.* **1989**, *101*, 663–672. [CrossRef]
34. Defant, M.J.; Maury, R.C.; Joron, J.-L.; Feigenson, M.D.; Leterrier, J.; Bellon, H.; Jacques, D.; Richard, M. The geochemistry and tectonic setting of the northern section of the Luzon arc (the Philippines and Taiwan). *Tectonophysics* **1990**, *183*, 187–205. [CrossRef]
35. Yang, T.F.; Lee, T.; Chen, C.-H.; Cheng, S.-N.; Knittel, U.; Punongbayan, R.S.; Rasdas, A.R. A double island arc between Taiwan and Luzon: Consequence of ridge subduction. *Tectonophysics* **1996**, *258*, 85–101. [CrossRef]
36. Bluth, G.J.S.; Doiron, S.D.; Schnetzler, C.C.; Krueger, A.J.; Walter, L.S. Global tracking of the SO_2 clouds from the June, 1991 Mount Pinatubo eruptions. *Geophys. Res. Lett.* **1992**, *19*, 151–154. [CrossRef]
37. Daag, A.S.; Dolan, M.T.; Laguerta, E.P.; Meeker, G.P.; Newhall, C.G.; Pallister, J.S.; Solidum, R.U. Growth of a postclimactic lava dome at Mount Pinatubo, July–October 1992. In *Fire and Mud: Eruptions and Lahars of Mount Pinatubo*; Newhall, C.G., Punongbayan, R.S., Eds.; University of Washington Press: Seattle, WA, USA, 1996; pp. 647–664.
38. Pallister, J.S.; Hoblitt, R.P.; Reyes, A.G. A basalt trigger for the 1991 eruptions of Pinatubo volcano? *Nature* **1992**, *356*, 426–428. [CrossRef]

39. Pallister, J.S.; Hoblitt, R.P.; Meeker, G.P.; Knight, R.J.; Siems, D.F. Magma mixing at Mount Pinatubo: Petrographic and chemical evidence from 1991 deposits. In *Fire and Mud: Eruptions and Lahars of Mount Pinatubo*; Newhall, C.G., Punongbayan, R.S., Eds.; University of Washington Press: Seattle, WA, USA, 1996; pp. 687–732.
40. Prouteau, G.; Scaillet, B. Experimental constraints on the origin of the 1991 Pinatubo dacite. *J. Petrol.* **2003**, *44*, 2203–2241. [CrossRef]
41. Heuret, A.; Lallemand, S. Luzon Arc Basemap. Scale 1:1,000,000. Basemap Generated by Betchaida Payot; using "Submap 4.1" 2005. Available online: http://www.submap.gm.univ-montp2.fr/maps-index.php (accessed on 1 November 2015).
42. Mercier, J.-C.C.; Nicolas, A. Textures and fabrics of upper-mantle peridotites as illustrated by xenoliths from basalts. *J. Petrol.* **1975**, *16*, 454–487. [CrossRef]
43. Barnes, S.J.; Roeder, P.L. The range of spinel compositions in terrestrial mafic and ultramafic rocks. *J. Petrol.* **2001**, *42*, 2279–2302. [CrossRef]
44. Ishii, T.; Robinson, P.T.; Maekawa, H.; Fiske, R. Petrological studies of peridotites from diapiric serpentinite seamounts in the Izu-Ogasawara-Mariana forearc, Leg 125. In *Proceedings of the Ocean Drilling Program Scientific Results 125*; Fryer, P., Pearce, J.A., Stokking, L.B., Eds.; Ocean Drilling Program: College Station, TX, USA, 1992; pp. 445–485.
45. Takahashi, E. Origin of basaltic magmas-implications from peridotite melting experiments and olivine fractionation model. *Bull. Volcanol. Soc. Jpn.* **1986**, *30*, S17–S40, (In Japanese with English abstract).
46. Yumul, G.P., Jr. Petrological characterization of the residual cumulate sequences of the Zambales Ophiolite Complex, Luzon, Philippines. *Ofioliti* **1989**, *14*, 253–291.
47. Sato, H. Nickel content of basaltic magmas: Identification of primary magmas and a measure of the degree of olivine fractionation. *Lithos* **1977**, *10*, 113–120. [CrossRef]
48. Arai, S. Petrological characteristics of the upper mantle peridotites beneath the Japan Island Arcs-Petrogenesis of spinel peridotites. *Geol. Geofiz.* **1991**, *32*, 8–26.
49. Wells, P.R.A. Pyroxene thermometry in simple and complex systems. *Contrib. Mineral. Petrol.* **1977**, *62*, 129–139. [CrossRef]
50. Ballhaus, C.; Berry, R.F.; Green, D.H. High pressure experimental calibration of the olivine-orthopyroxene-spinel oxygen geobarometer: Implications for the oxidation state of the upper mantle. *Contrib. Mineral. Petrol.* **1991**, *107*, 27–40. [CrossRef]
51. Bryndzia, L.T.; Wood, B.J.; Dick, H.J.B. The oxidation state of the Earth's sub-oceanic mantle from oxygen thermometry of abyssal spinel peridotites. *Nature* **1989**, *341*, 526–527. [CrossRef]
52. Morishita, T.; Hara, K.; Nakamura, K.; Sawaguchi, T.; Tamura, A.; Arai, S.; Okino, K.; Takai, K.; Kumagai, H. Igneous, alteration and exhumation processes recorded in abyssal peridotites and related fault rocks from an oceanic core complex along the Central Indian Ridge. *J. Petrol.* **2009**, *50*, 1299–1325. [CrossRef]
53. Blatter, D.L.; Carmichael, I.S.E. Hornblende peridotite xenoliths from central Mexico reveal highly oxidized nature of subarc upper mantle. *Geology* **1998**, *26*, 1035–1038. [CrossRef]
54. Parkinson, I.J.; Arculus, R.J. The redox state of subduction zones: Insights from arc-peridotites. *Chem. Geol.* **1999**, *160*, 409–423. [CrossRef]
55. Sun, S.-S.; McDonough, W.F. Chemical and isotopic systematics of oceanic basalts: Implications for mantle composition and processes. In *Magmatism in the Ocean Basins*; Saunders, A.D., Norry, M.J., Eds.; Geological Society London Special Publications: London, UK, 1989; Volume 42, pp. 313–345.
56. Johnson, K.T.M.; Dick, H.J.B.; Shimizu, N. Melting in the oceanic upper mantle: An ion microprobe study of diopsides in abyssal peridotites. *J. Geophys. Res.* **1990**, *95*, 2661–2678. [CrossRef]
57. Johnson, K.T.M.; Dick, H.J.B. Open system melting and temporal and spatial variation of peridotite and basalt at the Atlantis II Fracture Zone. *J. Geophys. Res.* **1992**, *97*, 9219–9241. [CrossRef]
58. Hellebrand, E.; Snow, J.E.; Dick, H.J.B.; Hofmann, A.W. Coupled major and trace elements as indicators of the extent of melting in mid-ocean-ridge peridotites. *Nature* **2001**, *410*, 677–681. [CrossRef] [PubMed]
59. Hellebrand, E.; Snow, J.E.; Hoppe, P.; Hofmann, A.W. Garnet-field melting and late-stage refertilization in 'residual' abyssal peridotites from the Central Indian Ridge. *J. Petrol.* **2002**, *43*, 2305–2338. [CrossRef]
60. Ross, K.; Elthon, D. Extreme incompatible trace-element depletion of diopside in residual mantle from south of the Kane F.Z. *Proc. Ocean Drill. Prog. Sci. Results* **1997**, *153*, 277–284.

61. Brunelli, D.; Seyler, M.; Cipriani, A.; Ottolini, L.; Bonatti, E. Discontinuous melt extraction and weak refertilization of mantle peridotites at the Vema lithospheric section (Mid-Atlantic Ridge). *J. Petrol.* **2006**, *47*, 745–771. [CrossRef]
62. Dick, H.J.B.; Natland, J.H. Late-stage melt evolution and transport in the shallow mantle beneath the East Pacific Rise. *Proc. Ocean Drill. Prog. Sci. Results* **1996**, *147*, 103–134.
63. Nixon, P.H. *Mantle Xenoliths*; John Wiley and Sons Ltd.: Great Britain, UK, 1987; 844p.
64. Arai, S.; Ishimaru, S.; Okrugin, V.M. Metasomatized harzburgite xenoliths from Avacha volcano as fragments of mantle wedge of the Kamchatka arc: Implication for the metasomatic agent. *Isl. ARC* **2003**, *12*, 233–246. [CrossRef]
65. Ishimaru, S.; Arai, S.; Ishida, Y.; Shirasaka, M.; Okrugin, V.M. Melting and multi-stage metasomatism in the mantle wedge beneath a frontal arc inferred from highly depleted peridotite xenoliths from the Avacha Volcano, Southern Kamchatka. *J. Petrol.* **2007**, *48*, 395–433. [CrossRef]
66. McInnes, B.I.A.; Gregoire, M.; Binns, R.A.; Herzig, P.M.; Hannington, M.D. Hydrous metasomatism of oceanic sub-arc mantle, Lihir, Papua New Guinea: Petrology and geochemistry of fluid-metasomatised mantle wedge xenoliths. *Earth Planet. Sci. Lett.* **2001**, *188*, 169–183. [CrossRef]
67. Gregoire, M.; McInnes, B.I.A.; O'Reilly, S.Y. Hydrous metasomatism of oceanic sub-arc mantle, Lihir, Papua New Guinea Part 2. Trace element characteristics of slab-derived fluids. *Lithos* **2001**, *29*, 91–108. [CrossRef]
68. Yumul, G.P., Jr. Ophiolite-hosted chromite deposits as tectonic setting and melting degree indicators: Examples from the Zambales ophiolite complex, Luzon, Philippines. *J. Resour. Geol. (Min. Geol.)* **1992**, *42*, 5–17.
69. Hawkins, J.W.; Evans, C.A. Geology of the Zambales Range, Luzon, Philippine Islands: Ophiolite derived from an island arc-back arc basin pair. In *The Tectonics and Geologic Evolution of Southeast Asian Seas and Islands*; Part 2; Hayes, D.E., Ed.; American Geophysical Union Monographs: Washington, DC, USA, 1983; Volume 27, pp. 95–123.
70. Rossman, D.L.; Castañada, G.C.; Bacuta, G.C. Geology of the Zambales ophiolite, Luzon, Philippines. *Tectonophysics* **1989**, *168*, 1–22. [CrossRef]
71. Evans, B.W.; Frost, B.R. Chrome-spinel in progressive metamorphism: A preliminary analysis. *Geochim. Cosmochim. Acta* **1975**, *39*, 959–972. [CrossRef]
72. Andal, E.S.; Arai, S.; Yumul, G.P., Jr. Complete mantle section of a slow-spreading ridge ophiolite: An example from the Isabela ophiolite in the Philippines. *Isl. ARC* **2005**, *14*, 272–294. [CrossRef]
73. Tamayo, R.A., Jr.; Maury, R.C.; Yumul, G.P., Jr.; Polve, M.; Cotton, J.; Dimalanta, C.B.; Olaguera, F.O. Subduction-related magmatic imprint of most Philippine ophiolites: Implications on the early geodynamic evolution of the Philippine archipelago. *Bull. Soc. Géol. Fr.* **2000**, *175*, 443–460. [CrossRef]
74. Deschamps, A.; Monié, P.; Lallemand, S.; Hsu, S.-K.; Yeh, K.H. Evidence for Early Cretaceous oceanic crust trapped in the Philippine Sea Plate. *Earth Planet. Sci. Lett.* **2000**, *179*, 503–516. [CrossRef]